Open Archive Toulouse Archive Ouverte (OATAO)

OATAO is an open access repository that collects the work of Toulouse researchers and makes it freely available over the web where possible

This is an author's version published in: **http://oatao.univ-toulouse.fr/20237**

Official URL: https://doi.org/10.1002/celc.201402153

Any correspondence concerning this service should be sent
to the repository administrator: tech-oatao@listes-diff.inp-toulouse.fr

Correlation of the Electrochemical Kinetics of High-Salinity-Tolerant Bioanodes with the Structure and Microbial Composition of the Biofilm

Raphael Rousseau,[a] Catherine Santaella,[c] Wafa Achouak,[c] Jean-Jacques Godon,[b] Anaïs Bonnafous,[b] Alain Bergel,*[a] and Marie-Line Délia[a]

Increasing the conductivity of the electrolytes used in microbial electrochemical systems is an essential prerequisite to large-scale application of these technologies. Microbial anodes formed on carbon felt from a salt marsh inoculum under polarisation at 0.1 V (versus a saturated calomel electrode), generated up to 85 A m^{-2} in media that contained 30–45 g L^{-1} of NaCl. Analyses of microbial populations showed a stringent selection of the two microbial genera *Marinobacter* and *Desulfuromonas*. Currents decreased if NaCl concentration was increased to 60 g L^{-1}. This highest salinity was shown to consistently impact the bioanode performance in three ways: voltammetry indicated degraded electron-transfer kinetics, confocal laser scanning microscopy showed a modified biofilm structure and DNA pyrosequencing detected a decrease in the level of *Desulfuromonas* spp. relative to *Marinobacter* spp. A consistent correlation was, thus, found between electrochemical kinetics, biofilm structure and the composition of the microbial community.

1. Introduction

Promising technologies have emerged in the last ten years, based on the newly discovered capability of microorganisms to catalyse the electrochemical oxidation of organic compounds.[1] Microbial fuel cells (MFCs) were the first of the microbial electrochemical systems (MESs), followed by the microbial electrolysis cells, that associate a microbial anode with an abiotic cathode for hydrogen evolution.[2] MESs have since bloomed into a wide variety of other devices in various application domains.[3,4] The development of these technologies depends, to a great extent, on efficient microbial anodes becoming available. Microbial anodes are most often composed of carbon or graphite,[5,6] on the surface of which an electroactive biofilm grows spontaneously. The optimisation of electroactive biofilms has consequently been the focus of much attention in the development of MESs.[7]

[a] Dr. R. Rousseau, Dr. A. Bergel, Dr. M.-L. Délia
Laboratoire de Génie Chimique
CNRS - University of Toulouse (INPT)
4 allée Emile Monso, BP 94234
31432 Toulouse (France)
E-mail: alain.bergel@ensiacet.fr

[b] Dr. J.-J. Godon, A. Bonnafous
Laboratoire de Biotechnologie de l'Environnement
INRA UR 0050
avenue des Etangs
11100 Narbonne (France)

[c] Dr. C. Santaella, Dr. W. Achouak
Laboratoire d'Ecologie Microbienne de la Rhizosphere &
Environnements Extrêmes
UMR 7265 CNRS - CEA - Aix Marseille Université
CEA Cadarache DSV/IBEB/SBVME
13108 Saint Paul lez Durance (France)
An invited contribution to a special issue on biofuel cells

The ionic conductivity of the electrolyte is one of the main parameters in any electrochemical process. If current flows through an electrochemical cell, a part of the electrical energy is lost through degradation into heat. This loss is proportional to the electrolyte resistance, that is, inversely proportional to electrolyte conductivity. Increasing the conductivity of the electrolyte is consequently a crucial objective in any electrochemical process. For example, hydrogen production by water electrolysis commonly uses KOH at concentrations as high as 33% by mass (pH above 14) to ensure a conductivity of 60 S m^{-1} (600 mS cm^{-1}). Even with such high conductivity, an inter-electrode distance of 2 cm and a current density of 300 A m^{-2} (common values for a medium-scale water electrolysis reactor) gives a non-negligible ohmic drop of 100 mV.

Increasing the ionic conductivity of the electrolyte has been an important objective for the development of MFCs, and more largely MESs. It has been confirmed experimentally that the addition of low concentrations of salts in an MFC improves its performance by reducing the internal resistance. For instance, increasing NaCl concentration from 5.8 to 23.4 g L^{-1} has been shown to increase the power density from 720 to 1330 mW m^{-2}.[8] Unfortunately, many microorganisms do not accept high salt concentrations, because they are sensitive to osmotic pressure. Consequently, above a certain threshold of salt concentration, the gain obtained by reducing the internal resistance of the reactor is lost by inhibiting the microbial catalysis. Lefebvre et al. have shown that the power produced by an MFC increased for NaCl concentrations up to 20 g L^{-1} only to decrease by 50% by 40 g L^{-1}.[9] There are, thus, two opposing objectives to be considered if designing MESs: to decrease energy losses by increasing conductivity and to respect the sensitivity of microorganisms to high salinities.

So far, most MFCs have been developed in solutions with low conductivities,[8–11] typically not exceeding 2 S m^{-1}.[12,13] In such conditions, a current density of 100 A m^{-2} flowing between electrodes 2 cm apart would cause an ohmic drop of 1000 mV. To put it bluntly, MFCs would provide only low current density if the conductivity of the electrolyte could not be increased considerably. To enlarge the applicability of MFCs, microbial anodes must become able to operate at high conductivities. This is an essential prerequisite if microbial electrochemical technologies are to advance.

Several ways of overcoming this obstacle have been put forward. Marine MFCs have been implemented in seas and oceans.[14,15] The seawater salinity of around 5.3 S m^{-1}, owing mainly to the NaCl concentration (35 g L^{-1}), is sufficient to transport the low currents produced, without a significant ohmic drop. Nevertheless, current densities produced by benthic MFCs remain modest, owing to the small number of organic compounds present in marine sediments.[16] Marine inocula have been tested in laboratory MFCs, either by adding acetate as a substrate[17,18] or by feeding the MFC with highly saline wastewaters.[19] These attempts have shown the feasibility of the systems but have not yet reached high current densities.

An alternative could be to implement pure strains isolated from marine environments, such as *Alteromonas litorea* sp. nov,[20] *Aestuariibacter aggregatus* sp. nov.,[21] *Ruegeria scottomollicae* sp. nov. and *Alteromonas genovensis* sp. nov.[22] Although *R. scottomollicae* sp. nov. and *A. genovensis* sp. have been isolated from electroactive biofilms, bacteria showing innate moderate halophily and strong electroactivity have not yet been described. *Geobacter sulfurreducens* (KN400), which is among the most widely investigated electroactive model strains, has been adapted to marine salinity with some success.[23] The halophilic strain *Geoalkalibacter subterraneus* has provided 3.3 A m^{-2} under polarisation at −0.2 V versus Ag/AgCl in a solution containing 17 g L^{-1} NaCl. To our knowledge, this is the highest current density that has been reached in saline conditions by a bioanode formed from a pure culture.[24]

A promising pathway has been recently opened up by using wild inoculum coming from a salt marsh.[25] The resulting microbial anodes have operated at electrolyte conductivities from 7.0 to 13.5 S m^{-1}, corresponding to NaCl concentrations from 30 to 60 g L^{-1}, respectively. Current densities up to 70 A m^{-2} have been reached at a NaCl concentration of 45 g L^{-1}. At 45 g L^{-1} NaCl, the solution conductivity is 10.4 S m^{-1}, which is around 1.5 times the conductivity of seawater; this represents a considerable advance with respect to the usual values of less than 2 S m^{-1} implemented in MESs.

Given the great technological hopes opened by such high-salinity-tolerant microbial anodes, the purpose of the present work was to characterise them. Two essential questions were addressed: "Are the high current densities related to the presence of specific microbial strains?" and "Does the salinity impact the biofilm structure and composition?"

Bioanodes were formed in three-electrode analytical set-ups under constant potential polarisation at 0.1 V versus a saturated calomel electrode (SCE) in solutions that contained very high NaCl concentrations (30–60 g L^{-1}). To characterise the bioanodes in well-defined conditions, kept as stable as possible, all experiments were performed in well-controlled electrochemical conditions with three-electrode set-ups under electroanalysis conditions (high solution volume and small electrode surface area). The electrochemical kinetics were assessed by numerical modelling, the biofilm structures were investigated by using several epifluorescent procedures coupled to confocal laser scanning microscopy and the microbial populations were compared by single strand conformation polymorphism (SSCP) and determined by DNA pyrosequencing. This multidisciplinary approach led to the first identification of a correlation between medium salinity, electrochemical performance, biofilm structure and biofilm microbial composition.

2. Results and Discussion

2.1. Bioanode Performance at Different Sodium Chloride Concentrations

2.1.1. Chronoamperometry

Bioanodes were formed on graphite felt under a constant applied potential of +0.1 V/SCE with acetate 40 mм. Three experimental runs were completed, each including three reactors containing different NaCl concentrations of 30, 45 and 60 g L^{-1}. The final electrolyte conductivities were 7.0, 10.4 and 13.5 S m^{-1}, respectively. A fourth experimental run was performed with three reactors at the same salinity of 45 g L^{-1}. All reactors gave similar current evolution (Figure 1 A). After a few days of initial lag time, the current increased with a sigmoidal evolution and reached a maximum plateau. For salinities of 30 and 45 g L^{-1} maximum current densities ranged from 16 to 85 A m^{-2} after around 15 days of polarisation. The highest salinity (60 g L^{-1} NaCl) led to lower current densities, ranging from 10 to 33 A m^{-2}.

The variability of the maximum currents from one reactor to another, illustrated for example by the triplicates of the fourth experimental run (Figure 2), has already been observed for experiments that use the same inoculum.[25] It has been attributed to the heterogeneity of the inoculum composition combined with the large amount used to inoculate (10% v/v). Such variability has already been reported in the literature if large amounts of wild inoculums are used.[26] Despite the experimental dispersion, analysis of the results showed the great interest of the inoculum for forming effective bioanodes at salinities of 30 and 45 g L^{-1}. Out of the nine reactors at these salinities, five gave current densities above 50 A m^{-2}, with maxima of 75 and 85 A m^{-2}, whereas the maximum values reported in the literature with similar graphite felt electrodes are 31[27] to 35 A m^{-2}.[12,28]

The polarisation was stopped as the current started to reach the maximum current for each reactor (Figure 1 A) in order to characterise the bioanodes at their maximum performance. After the polarisation was stopped it took about 10 min for the potential to reach a stable value, which was around −0.51 V/SCE for all bioanodes.
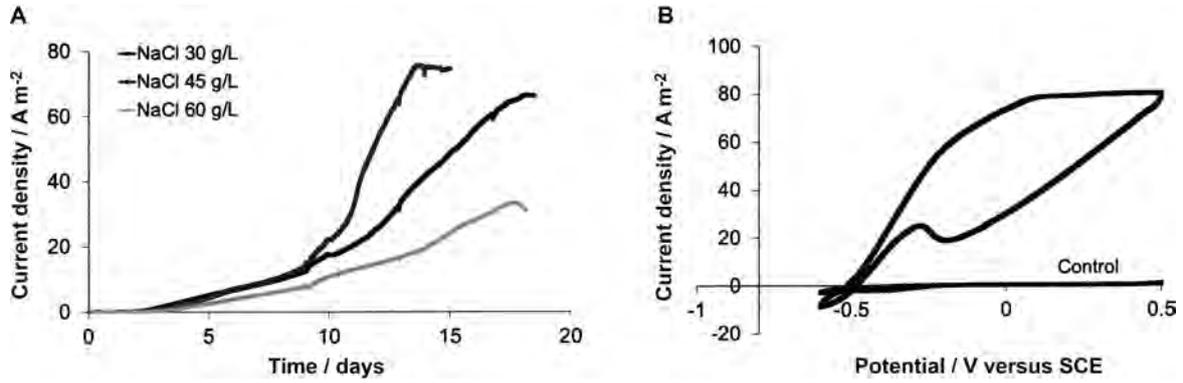
Figure 1. Electrochemical characteristics of bioanodes formed from a salt marsh sediment inoculum. A) Chronoamperometry at 0.1 V/SCE of three reactors run in parallel with three different NaCl concentrations (polarisation was stopped on the current reaching the maximum plateau). B) Cyclic voltammogram recorded at 1 m s^{-1} with the clean electrode just after inoculating (control) and at the end of the chronoamperometry for a NaCl concentration of 45 g L^{-1}.
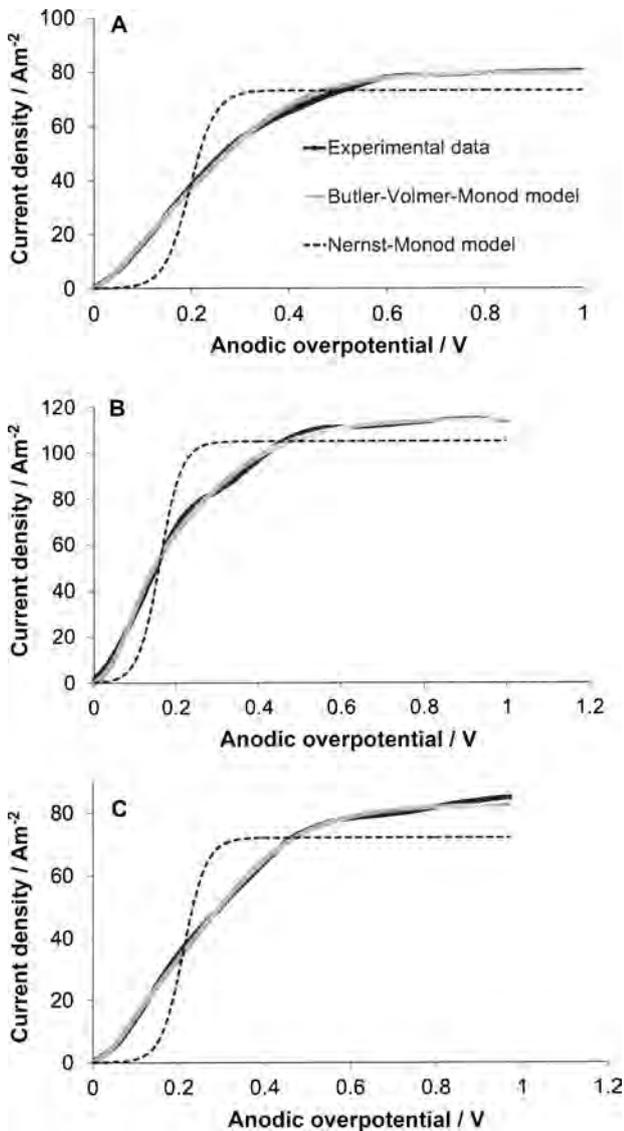

Figure 2. Forward scan (1 mV s^{-1}) voltammetry for three bioanodes formed in parallel by 25 days of polarisation at 0.1 V/SCE at a NaCl concentration of 45 g L^{-1} (triplicates). The experimental curves were plotted by taking the OCP as the origin of potentials and then fitted with the Nernst–Monod and the Butler–Volmer–Monod equations.

The formal redox potential of the HCO$_3^-$/CH$_3$COO$^-$ redox couple, shown in Equation (1):

$$CH_3COO^- + 4H_2O \rightarrow 2HCO_3^- + 9H^+ + 8e^- \tag{1}$$
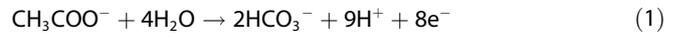
can be calculated according to the Nernst equation [Eq. (2)]:

$$E_{HCO_3^-/CH_3COO^-} = E^0_{HCO_3^-/CH_3COO^-} + \frac{R.T}{n.F}\ln\left(\frac{[HCO_3^-]^2.[H^+]^9}{[CH_3COO^-]}\right) \tag{2}$$

in which $n=8$ is the number of electrons produced per mole of acetate, $F=96485$ C.mol^{-1} is Faraday's constant, $R=8.314$ J mol^{-1} K^{-1} is the universal gas constant and $T=303$ K is the temperature. With the standard potential $E^0=0.187$ V/SHE at pH 7.5[29] and with $[CH_3COO^-]=0.04$ M, the formal potential can be expressed as [Eq. (3)]:

$$E_{HCO_3^-/CH_3COO^-} = -0.55 + \frac{R.T}{8.F}\ln([HCO_3^-]^2) \tag{3}$$

with respect to the saturated calomel reference electrode. The bicarbonate concentration had only a small impact on the formal potential value, which varied from -0.59 to -0.56 V/SCE for HCO$_3^-$ concentrations ranging from 5 to 100 mM. The open circuit potential (OCP) of -0.51 V/SCE was consequently close to the formal potential of the bicarbonate/acetate redox couple, which means that the intracellular and extracellular electron transports were driven by a small potential gradient. The biofilm formed on the bioanode surface demonstrated a great capability for electron transport from the intracellular acetate oxidation to the electrode surface.

2.1.2. Voltammetry

At the end of the experiments, once polarisation had been stopped and OCP was stable, cyclic voltammetry (CV) curves were recorded at 1 mV s^{-1}. The general shape of the CV curves was similar for all electrodes, independent of NaCl concentration. Large hysteresis was observed between the forward and

backward scans, which had different shapes (Figure 1B). The strong non-symmetry of the forward and backward curves indicated that the hysteresis phenomenon could not be attributed to a capacitive effect only, because capacitive currents are equal in both scanning directions. The forward potential scan (from OCP towards oxidation) induced a modification of the biofilm redox state so that the bioanode did not show the same behaviour on the backward (reductive) scan. Recording low-scan-rate CV curves affected the state of the bioanodes, which then needed several hours to recover their initial current production.

The forward CV curves were fitted numerically by two equations dedicated to microbial anodes. The Nernst–Monod equation[30] assumes a reversible (Nernstian) electron exchange between the biofilm and the electrode, whereas the Butler–Volmer–Monod equation[31] uses an irreversible Butler–Volmer law for the biofilm–electrode electron transfer. The Butler–Volmer–Monod equation gave a perfect fit for all CV curves, whereas the Nernst–Monod equation was not appropriate, as illustrated in Figure 2. The biofilm–electrode electron transfer was consequently not reversible. The Butler–Volmer–Monod equation expresses the current density (J) as a function of the potential (E) [Eq. (4)]:

$$J = J_{Max} \cdot \frac{1 - \exp\left(\frac{-n.F}{R.T}.\eta\right)}{K_1 . \exp\left(-\frac{(1-\alpha).n.F}{R.T}.\eta\right) + K_2 . \exp\left(\frac{-n.F}{R.T}.\eta\right) + \left(\frac{K_M}{S} + 1\right)} \quad (4)$$

in which J_{Max} (A m^{-2}) is the maximum current density, K_M (mol L^{-1}) is the substrate affinity constant, S (mol L^{-1}) is the substrate concentration, α is the charge transfer coefficient and K_1 and K_2 are dimensionless parameters.

Five parameters must be adjusted: J_{Max}, K_M, α, K_1 and K_2. The value of K_M was taken to be constant and equal to 5 mM to decrease the number of parameters to be adjusted numerically. This value corresponded to the acetate concentration from which a clear decrease of current was observed during the chronoamperometries; it was of the same order of magnitude as that reported in the literature (2.2 mM).[31] The other four parameters were adjusted by fitting the experimental voltammograms through least squares regression.

According to Hamelers et al., who designed Equation (4),[31] the K_1 parameter represents how fast the biochemical reaction runs relative to the electrochemical reaction, that is, the ratio of the limiting biochemical current density to the electrochemical exchange current density. Theoretically, if the electrochemical reaction was extremely fast, K_1 would tend to zero and the Butler–Volmer–Monod equation would approach the Nernst–Monod equation. Here, K_1 varied from 4.0 to 18.8. These values, always greater than 3, indicated that the electron transfer was far from reversible (Nernstian) and that the electrochemical reaction was considerably slower than the biochemical reaction.

In the Butler–Volmer–Monod approach, the metabolic part is represented by a two-step reaction that forms an intermediate complex, similar to enzymatic mechanisms. K_2 describes the ratio of the forward reaction, from the intermediate complex to the product, over the backward reaction, from the intermediate complex to the substrate. The forward rate from the complex to the product should be higher than the backward rate, because microorganisms need to degrade the substrate to obtain energy to grow. The K_2 value is consequently expected to be larger than 1. This was confirmed here, with K_2 ranging from 31 to 295, without direct correlation to the NaCl concentration of 60 g L^{-1}. The large range of K_2 values may indicate some diversity in the metabolic behaviour of the bioanodes.

The J_{Max} and α parameters distinguished two groups of NaCl concentrations. At the lower NaCl concentrations (30 and 45 g L^{-1}), J_{Max} values ranged from 93 to 134 A m^{-2} but decreased to 57 A m^{-2} at the highest concentration (60 g L^{-1}). The average α was 0.78 ± 0.03 g L^{-1} at lower concentrations and increased to 0.88 at 60 g L^{-1}. Values of α generally lie between 0.3 and 0.7 for most electrochemical reactions.[32] In the bioelectrochemical domain, an α value of 0.43 has been found for a biocathode formed with *Geobacter sulfurreducens*[33] and 0.42–0.45 for protein electrochemistry.[34,35] The high values obtained here are not usual, but have been reported in protein electrochemistry.[36] They point to a very dissymmetric energy barrier in the electron-transfer process, which hindered electron transfer to the electrode and was enhanced at high salinity. The higher value of α coupled with the lower value of J_{Max} indicated that a NaCl concentration of 60 g L^{-1} was detrimental to the electrode/biofilm electron-transfer step.

In summary, CV analyses showed that the global reaction rate was controlled by the electrode/biofilm electron-transfer rate (K_1 higher than three, high values of α) and the highest salinity decreased this electron-transfer rate (higher value of α, decrease in J_{max}). The metabolic behaviour varied widely (large range of K_2 values).

2.2. Biofilm Morphology

At the end of polarisation at 0.1 V/SCE, bioanodes were extracted from the reactors and imaged by epifluorescence (Figure 3) and confocal laser scanning microscopy (Figure 4) to take advantage of the complementary views given by the two techniques. In optical epifluorescence microscopy, the fluorescence is emitted by the sample, through the whole excited volume; this leads to images with a large depth of field but masks the resolution of structures in the focal plane. Confocal microscopy allows a series of virtual thin optical sections to be acquired, free from background light coming from planes away from the focal one. Much more detail is observed but usually only the shallowest portions of the sample are examined.

Biofilms were stained with NanoOrange reagent, which shows up the biofilm matrix as well as the cells (Figure 3 and Figure 4 d–f). In some electroactive biofilms, the association of Gram-positive and Gram-negative bacteria has led to better electroactivity than would be produced by the strains alone.[37] Consequently we analysed the structure of electroactive biofilms with Bacterial Gram staining, a labelling process allowing the Gram status to be assessed (Figure 4 a–c).
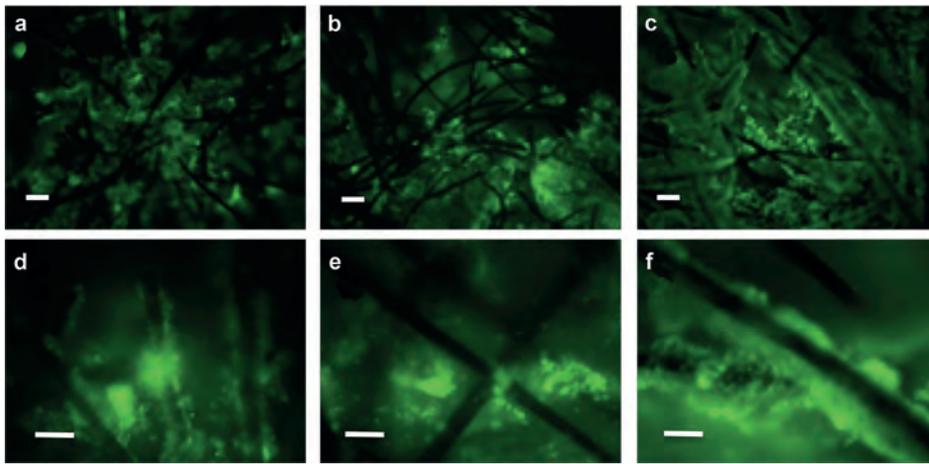
Figure 3. Bioanodes stained with NanoOrange to localise proteins in the exopolymer matrix. Epifluorescence objective x10 (a–c) and x40 (d–f). Bioanodes were formed at NaCl concentrations of 30 g L^{-1} (a, d), 45 g L^{-1} (b, e) and 60 g L^{-1} (c, f). Scale bars: 20 µm. Increasing the NaCl concentration intensified cladding of graphite fibres.
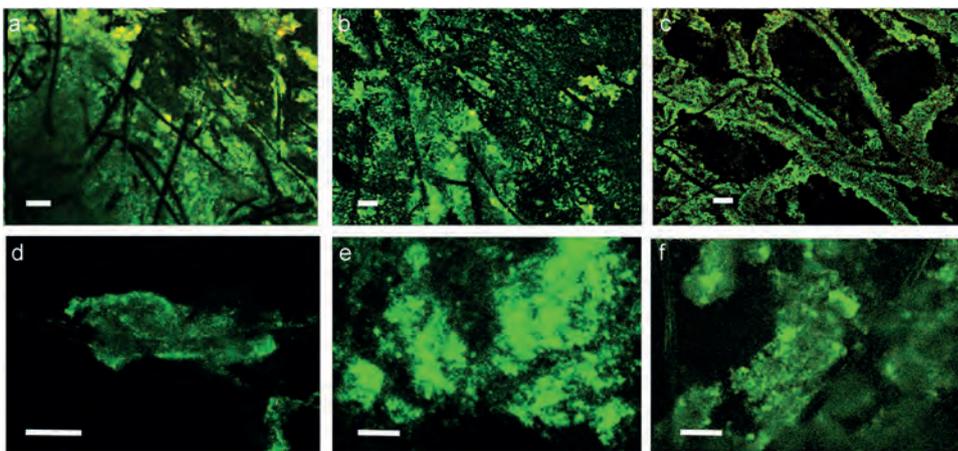

Figure 4. Confocal laser scanning microscope images of bioanodes stained with Bacterial Gram staining (a–c) and NanoOrange (d–f). Bioanodes were formed at NaCl concentrations of 30 g L^{-1} (a, d), 45 g L^{-1} (b, e) and 60 g L^{-1} (c, f). Scale bars: 20 µm. Projection of Z sections (1 µm step) through a) 25 µm, b) 46 µm, c) 1 µm, d) 21 µm, e) 22 µm and f) 17 µm. Sheathing of fibres increased with increasing NaCl concentration and the biofilm became more rarefied in the interstitial spaces between adjacent graphite fibres.

developed in the interstitial spaces between graphite fibres (Figure 3 a, b, d, e and Figure 4 a, b, d, e). Increasing NaCl concentration to 60 g L^{-1} strengthened the biofilm as a sheath cladding the fibres of the graphite felt (Figure 3 c, f and Figure 4 c, f) and confocal microscopy confirmed that no biofilm formed in the interstices between fibres: the interfibre areas were dark (Figure 4 c).

In the domain of electroactive biofilms, few studies have described the relationships between the structure of biofilms and their electrochemical characteristics. Read et al. have shown that biofilms formed from cocultures of *Enterococcus faecium*, a Gram-positive bacterium, and Gram-negative strains segregate over time.[37] This segregation may be an essential difference in strategy for electron transfer (Gram-negative) and substrate capture (Gram-positive). In bioanodes made from *Geobacter sulfurreducens*, the structural organisation of the biofilm was responsive to the electron donor.[38] Bioanodes formed with formate and lactate had smaller thickness and electrode coverage and higher roughness compared with those fed with acetate.
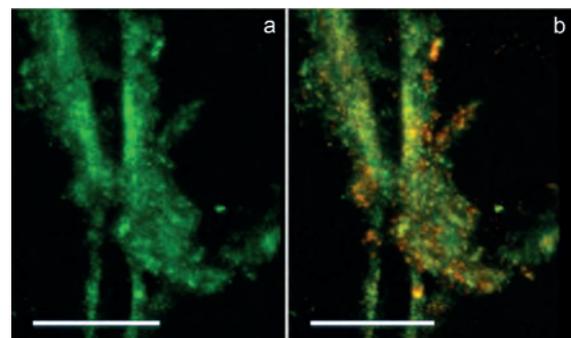
In both epi- and confocal microscopy, felt fibres that were not covered with stained biofilms appeared as dark strings. At the highest magnification (x100) an analysis of Gram staining indicated the presence of Gram-positive cells as individuals within biofilms composed mainly of Gram-negative bacteria (Figure 5). At a magnification that showed a broad outline of the biofilm structure (Figure 4 a–c), the implication of Gram-positive cells was weakened by the abundance of Gram-negative cells. Increasing NaCl concentration from 30 to 45 and 60 g L^{-1} tended to reduce the density of Gram-positive bacteria (red-stained bacteria, Figure 4 a–c).

Bacterial Gram stain and NanoOrange reagent label different structures in biofilms: cells or cells together with the exopolymer matrix, respectively. Both stains brought out consistent features on the biofilm structure according to NaCl concentration. Two different kinds of biofilm structure were differentiated depending on the salinity. For NaCl concentrations of 30 and 45 g L^{-1}, biofilms covered the fibres discontinuously and

Figure 5. Confocal laser scanning microscope images of bioanodes stained with Bacterial Gram staining (SYTO 9 and hexidium iodide). Bioanodes were formed at a NaCl concentration of 30 g L^{-1}. Scale bars: 50 µm. Projection of Z sections (1 µm step) through 36 µm. a) SYTO 9 fluorescence and b) superimposed fluorescences of SYTO 9 and hexidium iodide. High magnification suggested the presence of Gram-positive cells in a biofilm of Gram-negative bacteria.
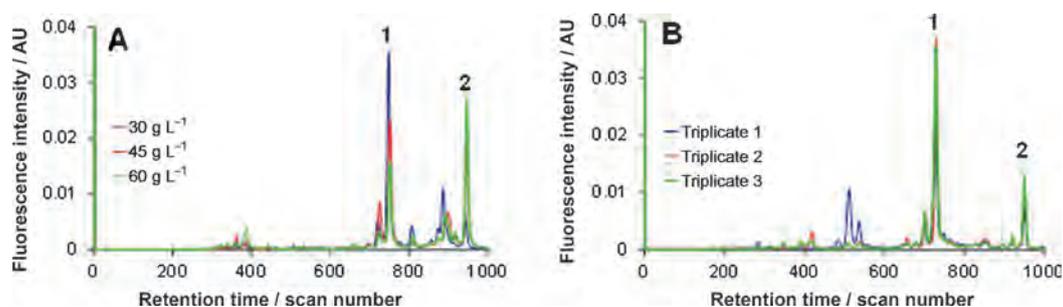
Figure 6. Comparison between SSCP profiles of bioanode bacterial communities formed A) at different NaCl concentrations and B) at the same NaCl concentration of 45 g L^{-1}. The fluorescence intensity (arbitrary unit) and the retention time (scan number) depend on the equipment and can be used only to compare different samples in exactly the same conditions.

Metabolic constraints associated with these electron donors prevented optimal biofilm growth and decreased the performance of the anode. The biofilm morphology has also been shown to control the performance of *Geobacter sulfurreducens* biocathodes.[33] Nevertheless, to the best of our knowledge, no data in the literature have addressed the impact of salinity on the structure of electroactive biofilms.

Setting aside electrochemical considerations, some works have dealt with the impact of NaCl, or more generally ionic strength, on biofilm formation and architecture. In aquatic environments, strains of *Vibrio fisheri*, a moderately halophilic bacterium, become biofilm producers at salinity concentrations in the 10–50 g L^{-1} range, whereas significantly less biofilm is formed at higher salinities (60–90 g L^{-1}).[39] Several rhizobacteria, associated with the rhizosphere of *Salicornia* growing in hypersaline soils, show maximal biofilm formation at 1 M salt concentration.[40] Salinity induces the formation of exopolymeric substances, which promote root colonisation by bacteria. Salinity has also been shown to enhance biofilm formation on *Staphylococcus epidermis* through the activation of the sigB operon.[41] Recently, Janjaroen et al. monitored the attachment of *Escherichia coli* onto clean PVC surfaces.[42] They observed that both cell adhesion and biofilm roughness increased with ionic strength (3–10 mM KCl), and suggested that the physical structure of biofilms could facilitate the adhesion of *E. coli* cells.

In summary, data from the literature show that salinity is a factor that favours biofilm formation in general and that, in the bioelectrochemical domain, biofilm structure can strongly influence the electrochemical characteristics of bioanodes and biocathodes. It was shown here, for the first time, that salinity stress (60 g L^{-1} NaCl) decreased the current generated by bioanodes by acting on biofilm structure. The lower current density provided at the highest salinity corresponded to a restricted structure of the biofilm, which was rarefied in the interstitial spaces but formed sheaths around the fibres.

2.3. Analysis of Microbial Communities

2.3.1. Microbial Communities on Bioanodes

The microbial composition of the bioanode was analysed by SSCP. In this fingerprint technique, each peak corresponds to a major phylotype in the microbial community. All SSCP profiles showed low diversity with two major peaks, independent of salinity (peaks 1 and 2 in Figure 6). The similarity among microbial populations was even more clear for bioanodes formed at the same salinity from the same inoculum sample (triplicates, Figure 6B). The poor reproducibility observed on current densities (see Section 3.1) was consequently not related to differences in the dominant members of the microbial communities.

SSCP fingerprinting and 16S rDNA pyrosequencing both revealed the same low level of richness (Figure 7). All pyrosequenced bacteria belonged to the phyla of delta- and epsilon-Proteobacteria. At all NaCl concentrations, more than 90% of the microbial population was made up of two phylotypes: *Marinobacter spp* and *Desulfuromonas spp*, thus confirming the two major peaks observed on the SSCP profiles. The relative abundances of these genera were similar for NaCl concentrations of 30 and 45 g L^{-1} with a *Marinobacter-Desulfuromonas* ratio close to 2:1 (Figure 7 A, B). For the highest salinity, the *Desulfuromonas* genera represented only 6% of the microbial population, against 89% for *Marinobacter* (Figure 7 C). High salinity was clearly detrimental to *Desulfuromonas* but the decrease of *Desulfuromonas* at 60 g L^{-1} was balanced fully by the *Marinobacter* increase. Other bacteria, each of which made up less than 1%, belonged to various families including *Alteromonadaceae* and *Deferribacterriacae*.

The presence of the *Desulfuromonas* genus was not surprising, as these bacteria had already been identified as electroactive in the pioneering MFC studies.[43] This genus has been found to be dominant on bioanodes formed from marine sediments[44,45] and other different types of inoculum, such as paper-mill effluents.[46] *Desulfuromonas acetoxidans* is known to reduce Fe^{III} oxides through outer-membrane type-C cytochromes[47] and it has been implemented in MFCs.[48]

In contrast, the *Marinobacter* genus has not yet been detected as one of the dominant species of electroactive biofilms. To the best of our knowledge, this is the first time it has been shown to be dominant in microbial anodes. This genus is known to produce siderophores. Siderophores are Fe^{III} chelators produced by microorganisms to solubilise iron, particularly in conditions of low iron concentration.[49] The dominance of the two iron reducing Proteobacteria observed here was consistent with the fairly high concentration of iron contained in
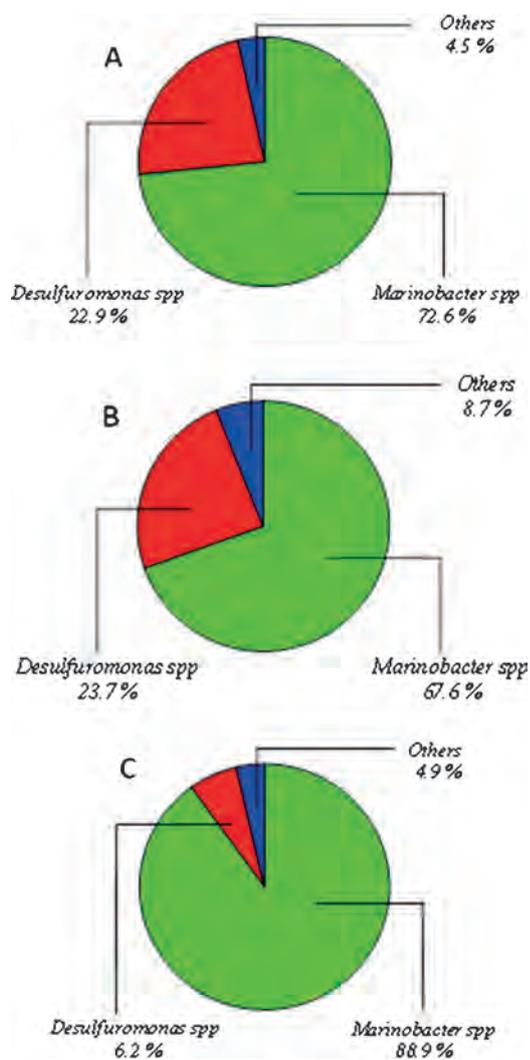
Figure 7. Composition of the bioanode bacterial communities formed at NaCl concentrations of A) 30 g L^{-1}, B) 45 g L^{-1} and C) 60 g L^{-1}.
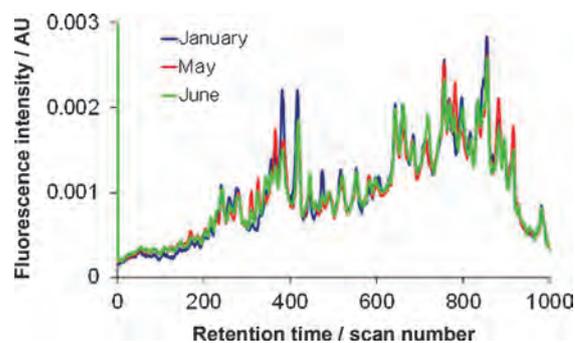

Figure 8. SSCP profiles of salt marsh inoculum at different storage times. The fluorescence intensity (arbitrary unit) and the retention time (scan number) depend on the equipment and can be used only to compare different samples in exactly the same conditions.

salt marsh inoculum [2.1 ± 0.5 percentage by mass measured by selected area electron diffraction (SAEDX)]. Moreover, the literature on electroactive bacteria has established a strong correlation between electroactivity and the ability to reduce insoluble metals such as Fe^{III} and Mn^{IV} in natural environments.[50]

2.3.2. Microbial Population of the Inoculum

In contrast to the microbial communities that composed the bioanodes, the microbial population of the salt marsh inoculum revealed a large diversity with more than 30 peaks detected by SSCP (Figure 8) and a low relative abundance of each species. The large biodiversity contained in salt marsh sediments was not surprising as sediments have already been reported to contain a very diverse microbial community.[51] The microbial composition of the inoculum showed good stability during six months of storage and, in particular, no spontaneous selection of a given phylotype occurred (Figure 8). Abundances of *Desulfuromonas* and *Marinobacter* in the inoculum

always remained small, in the range of 0.2 to 1.3% for both species. The low level of these two genera in the inoculum highlighted the stringent selection that occurred during bioanode formation. Moreover, this selection was reproducible in each bioanode, always resulting in the same ratio of the two dominant species, except for at the highest salinity. It can be concluded that only a restricted number of the species present in the inoculum were able to take advantage of the electrode to grow.

The similarity of the dominant species in the bioanodes formed at 30 and 45 g L^{-1} should be emphasised (Figures 7 A and 7 B) and combined with the remarkable stability of microbial composition of the inoculum during six months of storage (Figure 8). Consequently, the poor reproducibility of the currents generated by the bioanodes cannot be attributed to the variability of the microbial composition of the inoculum or to a difference in the bioanode microbial communities.

Two suppositions can be made to explain the variability from one reactor to the other. First, some species present in minor percentages in the bioanode communities might play a significant role in current production. This means that despite their low ratio, any small variation from one bioanode to the other could induce large differences in currents. Secondly, spatial heterogeneities in the chemical composition of the inoculum can also be evoked. For instance, the measurements of iron by SAEDX at different spots revealed significant differences. Finally, the biofilm construction may be a source of variability, as selecting dominant species from so large an initial biodiversity is an erratic process.

2.4. General Discussion

Bioanodes formed on graphite felt with a salt marsh inoculum produced considerable current densities, generally higher than 50 and up to 85 A m^{-2} at an applied potential of 0.1 V/SCE. These bioanodes had the advantage of operating at NaCl concentrations of 30–45 g L^{-1}, which ensured ionic conductivities of 7.0 and 10.4 S m^{-1}. Increasing NaCl concentration to 60 g L^{-1} (conductivity 13.5 S m^{-1}) reduced the current density, which nevertheless remained above 10 A m^{-2}. OCPs were low, around −0.51 V/SCE, which is one of the hallmarks of efficient bioano-

des. Analysis of voltammetry data showed that electron transfer from the biofilm to the electrode was a rate-limiting step. Its kinetics was far from reversible and the increase of salinity at 60 g L^{-1} had a detrimental effect.

The lower electrochemical performance obtained at a NaCl concentration of 60 g L^{-1} was correlated to a modification of the biofilm structure. The biofilm no longer grew in the interstitial spaces between the graphite fibres, as was the case with NaCl concentrations of 30 and 45 g L^{-1}, but formed sheaths only around the fibres. The microbial communities of the bioanodes were essentially made up of *Marinobacter spp.* and *Desulfuromonas spp.*, with a ratio close to 2:1 at NaCl concentrations of 30 and 45 g L^{-1}. The highest salinity decreased the proportion of *Desulfuromonas* to 6% against 89% for *Marinobacter*. The increase of the proportion of *Marinobacter* at high salinity is consistent with the known high halotolerance of some species. For instance, *Marinobacter hydrocarbonoclasticus* is able to grow in NaCl concentrations of up to 204.75 g L^{-1} (3.5 M).[52]

The decrease in the bioanode performance at the highest salinity was correlated with changes in the biofilm architecture and a modification in the relative abundance of the two dominant species. The modification of the biofilm structure, which tended to decrease the biofilm surface area exposed to the solution and to decrease cell density, was consistent with the decrease in the current produced. The presence of *Desulfuromonas* strains was probably related to the production of current, the electroactive capability of these genera spp is already known. Its weaker presence in the bioanodes formed at high salinity was also consistent with lower electrochemical performance. This is the first time to our knowledge that such a correlation between voltammetry, biofilm structure and microbial composition has been demonstrated to explain the behaviour of microbial bioanodes.

The precise role of *Marinobacter* spp. now has to be identified by further investigations. Two different assumptions can be made. On the one hand, *Marinobacter* strains may be involved directly in the electron production and transfer processes. On the other hand, they may be useful in the biofilm construction. If *Marinobacter* spp. were not involved directly in electron production and transfer, but only in biofilm construction, this would explain why biofilms with a high proportion of *Marinobacter* spp. produced lower currents. Nevertheless, *Marinobacter* spp. must find some advantage in contributing to electroactive biofilms; why else would it be selected systematically from initial media containing so great a microbial diversity in which the abundance of *Marinobacter* spp was low? This question should be an interesting topic for further investigations.

3. Conclusions

Efficient microbial anodes were formed in electrolytes that contained 30–45 g L^{-1} NaCl. The design of these bioanodes, which are able to produce up to 85 A m^{-2} in electrolytes with more than 100 mS cm^{-1} conductivity, should considerably contribute to the development of microbial electrochemical technologies. The efficiency of the bioanodes at such high salinities correlated to the selection of the two microbial genera *Marinobacter* and *Desulfuromonas*. At the highest salinity (60 g L^{-1} NaCl) the bioanode performance was affected, owing to modification of the biofilm structure and a decrease in the percentage of *Desulfuromonas* spp. relative to that of *Marinobacter* spp.

The reproducible, stringent selection of these two genera from a large diverse range of microbial genera revealed their particular capability to form electroactive biofilms in highly saline electrolytes. The *Desulfuromonas* species have already been identified as electroactive; the precise role of *Marinobacter* remains to be determined. These two genera show promise for the development of efficient bioanodes in highly conductive electrolytes.

Experimental Section

Media

Sediment was collected from a salt marsh of the mediterranean sea (Gruissan, France). The pH of the water was 6.5–7.4 and its conductivity 7.6–12.3 S m^{-1}, that is, up to 2.3 times the conductivity of seawater (5.3 S m^{-1}). Salt marsh sediments were analysed after drying by using SAEDX (Oxford detector) with a scanning electron microscope (Leo 436 VP). Different samples were dried and each sample was analysed at several places, which gave the identical spectra.

The culture medium contained NH$_4$Cl (2 g L^{-1}), K$_2$HPO$_4$ (0.5 g L^{-1}), sodium acetate 40 mM, HCl (37%; 46 mL), MgCl$_2$·6H$_2$O (55 mg L^{-1}), FeSO$_4$(NH4)$_2$SO$_4$·6H$_2$O (7 mg L^{-1}), ZnCl$_2$·2H$_2$O (1 mg L^{-1}), MnCl$_2$·4H$_2$O (1.2 mg L^{-1}), CuSO$_4$·5H$_2$O (0.4 mg L^{-1}), CoSO$_4$·7H$_2$O (1.3 mg L^{-1}), BO$_3$H$_3$ (0.1 mg L^{-1}), Mo$_7$O$_2$(NH4)$_6$·4H$_2$O (1 mg L^{-1}), NiCl$_2$·6H$_2$O (0.05 mg L^{-1}), Na$_2$SeO$_3$·5H$_2$O (0.01 mg L^{-1}) and CaCl$_2$.2H$_2$O (60 mg L^{-1}). Solutions were complemented with three different NaCl concentrations (30, 45 and 60 mg L^{-1}). The pH was 7.5, which is close to that of the natural environment of the inoculum, and this value did not change during the chronoamperometries.

Electrodes and Electrochemical Procedure

Anodes were made of graphite felt (Mersen, Gennevilliers, France) of 2 cm^2 projected surface area and current densities were expressed with respect to this projected surface area. 254SMO grade stainless steel (Outokumpu, Avesta, Sweden) was used as the counter electrode, because of its resistance to corrosion in chloride solutions. Working and counter electrodes were connected to the electrical circuit by titanium wires (Alfa Aesar, Schiltigheim, France), which were insulated with a heat shrinkable sheath. SCEs (Radiometer, SCE) were used as references (potential 0.241 V/SHE) and potentials were monitored by using a multi-channel potentiostat (Bio-Logic SAS, Claix, France). Each reactor, equipped with a three-electrode system, was filled with 50 mL raw salt marsh sediment and 450 mL of culture medium. The reactors were placed in thermostatic baths maintained at 30 °C. Each reactor was hermetically closed, the 200 mL headspace was deoxygenated by nitrogen bubbling for 20 min and the graphite felt anode (working electrode) was then polarised at +0.1 V/SCE (chronoamperometry).

Each experimental run was performed with three independent reactors inoculated with the same inoculum sample and operated in parallel at the same time. During polarisation, on a decrease of the

current the acetate concentration was measured (enzyme kit K-ACETAK, Megazyme, (Libios) Pontchara sur Turdine, France) and acetate was added to recover the 40 mM initial concentration. CV curves were recorded at the end of the chronoamperometries. Three successive cycles were performed between −0.6 and 0.5 V/SCE. The second and third cycles were generally perfectly superimposed, so only the third cycle is reported here.

Electrode Preparation for Epifluorescence Microscopy

A section (0.5×0.5 cm^2 and less than 0.5 cm thick) was sliced from the surface of the electrode. The sample was labelled with Bacterial Gram stain (Invitrogen, Carlsbad, CA, USA or NanoOrange reagent (Invitrogen; x25) according to the recommendations of the manufacturer. NanoOrange reagent is virtually non-fluorescent in aqueous solution but undergoes a dramatic fluorescence enhancement upon interaction with proteins. It enables the biofilm matrix to be detected, together with the cells. Bacterial Gram stain is based on the SYTO 9 stain, which labels both Gram-positive and Gram-negative bacteria, and hexidium iodide, which crosses the membrane of Gram-positive cells and removes SYTO 9. Gram-negative bacteria fluoresce green and gram-positive bacteria fluoresce red. Dead cells stain variably.

The samples were mounted between a slide and a CoverWell incubation chamber (Invitrogen; 0.5–2 mm thickness). A Fluo View Olympus CLSM microscope equipped with a krypton–argon laser (488, 568 and 647 nm lines) and objectives LCPPlan 10/XX and LCPlanFL 40/0.60 (working distance 2.3 mm) were used for microscopic observations. Emissions were observed with appropriate filters (510–560 nm on the green channel, 585–640 nm on the red channel). Image stacks were collected every 1 μm. Z-stacks were generated by using the Fluo View software. Epifluorescence was recorded on an Olympus camera. Three to five random fields were examined by using x10, x40 and x100 objectives. GraphicConverter X and PowerPoint were used for the treatment of images.

Electrode Storage, DNA Extraction for SSCP Fingerprinting and DNA Sequencing

To avoid any deviation of the microbial community between the end of the experiment and the analysis, a piece of each electrode was taken at the end of each chronoamperometry and stored at −80 °C in a 2 mL tube (Eppendorf) until DNA extraction was performed. Genomic DNA was extracted and purified from the piece of graphite felt sample by using a protocol described previously.[53] The total DNA extracted was purified by using a QiAmp DNA microkit (Qiagen, Hilden, Germany). DNA amount and purity of extracts were confirmed by spectrophotometry (Infinite NanoQuant M200, Tecan, Austria). The bacterial communities of biofilms were analysed by the polymerase chain reaction (PCR)-SSCP fingerprint technique and pyrosequencing. For SSCP, the highly variable V3 regions of 16S rRNA gene were amplified by PCR from each biofilm DNA sample.

One microlitre of genomic DNA sample was amplified by using the primers w49 (5′-ACGGTCCAGACTCCTACGGG-3′, Escherichia coli position F330) and 5′-6FAM labelled w104 (5′-TTACCGCGGCTGCTGCTGGCAC-3′, E. coli position R533)[54] in accordance with the capillary electrophoresis finger print technique (CE-SSCP) amplification methods previously described.[55] CE-SSCP electrophoresis was performed with ABI310 (Applied Biosystems)[55] CE-SSCP profiles were analysed by using GeneScan software (Applied Biosystems) and the 'StatFingerprints' package.[56] Pyrose-

quencing of the DNA samples by using a 454 protocol was performed by the Research and Testing Laboratory (Lubbock, USA).

[1] B. E. Logan, *Nat. Rev. Microbiol.* **2009**, *7*, 375–381.
[2] B. E. Logan, D. Call, S. Cheng, H. V. M. Hamelers, T. H. J. A. Sleutels, A. W. Jeremiasse, R. A. Rozendal, *Environ. Sci. Technol.* **2008**, *42*, 8630–8640.
[3] D. Pant, A. Singh, G. Van Bogaert, S. I. Olsen, P. S. Nigam, L. Diels, K. Vanbroekhoven, *RSC Adv.* **2012**, *2*, 1248–1263.
[4] T. H. J. A. Sleutels, A. Ter Heijne, C. J. N. Buisman, H. V. M. Hamelers, *ChemSusChem* **2012**, *5*, 1012–1019.
[5] A. Rinaldi, B. Mecheri, V. Garavaglia, S. Licoccia, P. Di Nardo, E. Traversa, *Energy Environ. Sci.* **2008**, *1*, 417–429.
[6] Y. Qiao, S.-J. Ba, C. M. Li, *Energy Environ. Sci.* **2010**, *3*, 544–553.
[7] P. Borole, G. Reguera, B. Ringeisen, Z.-W. Wang, Y. Fengd, B. H. Kim, *Energy Environ. Sci.* **2011**, *4*, 4813–4834.
[8] H. Liu, S. Cheng, B. E. Logan, *Environ. Sci. Technol.* **2005**, *39*, 5488–5493.
[9] O. Lefebvre, Z. Tan, S. Kharkwal, H. Y. Ng, *Bioresour. Technol.* **2012**, *112*, 336–340.
[10] Y. Feng, X. Wang, B. E. Logan, H. Lee, *Appl. Microbiol. Biotechnol.* **2008**, *78*, 873–880.
[11] Y. Mohan, D. Das, *Int. J. Hydrogen Energy* **2009**, *34*, 7542–7546.
[12] D. Pocaznoi, B. Erable, L. Etcheverry, M.-L. Delia, A. Bergel, *Phys. Chem. Chem. Phys.* **2012**, *14*, 13332–13343.
[13] B. E. Logan, K. Rabaey, *Science* **2012**, *337*, 686–690.
[14] L. M. Tender, S. A. Gray, E. Groveman, D. A. Lowy, P. Kauffman, J. Melhado, R. C. Tyce, D. Flynn, R. Petrecca, J. Dobarro, *J. Power Sources* **2008**, *179*, 571–575.
[15] M. E. Nielsen, C. E. Reimers, H. K. White, S. Sharma, P. R. Girguis, *Energy Environ. Sci.* **2008**, *1*, 584-593.
[16] B. E. Logan, *Microbial Fuel Cells*, John Wiley & Sons, New York, **2008**, ch. 10, p. 163.
[17] B. Erable, M. A. Roncato, W. Achouak, A. Bergel, *Environ. Sci. Technol.* **2009**, *43*, 3194–3199.
[18] C. Dumas, A. Mollica, D. Feron, R. Basseguy, L. Etcheverry, A. Bergel, *Bioresour. Technol.* **2008**, *99*, 8887–8894.
[19] S. J. You, J. N. Zhang, Y. X. Yuan, N. Q. Ren, X. H. Wang, *J. Chem. Technol. Biotechnol.* **2010**, *85*, 1077–1083.
[20] J. H. Yoon, S. H. Yeo, T. K. Oh, Y. H. Park, *Int. J. Syst. Evol. Microbiol.* **2004**, *54*, 1197–1201.
[21] Y. Wang, H. Wang, J. W. Liu, Q. L. Lai, Z. Z. Shao, B. Austin, X. H. Zhang, *FEMS Microbiol. Lett.* **2010**, *309*, 48–54.
[22] I. Vandecandelaere, O. Nercessian, E. Segaert, W. Achouak, A. Mollica, M. Faimali, P. De Vos, P. Vandamme, *Int. J. Syst. Evol. Microbiol.* **2008**, *58*, 2589–2596.
[23] K. P. Nevin, P. Zhang, A. E. Franks, T. L. Woodard, D. R. Lovley, *J. Power Sources* **2011**, *196*, 7514–7518.
[24] J. P. Badalmenti, R. Krajmalnik-Brown, C. I. Torres, *mBio* **2013**, *4*, e00144-13.
[25] R. Rousseau, X. Dominguez-Benetton, M.-L. Delia, A. Bergel, *Electrochem. Commun.* **2013**, *33*, 1–4.
[26] D. A. Finkelstein, L. M. Tender, J. G. Zeikus, *Environ. Sci. Technol.* **2006**, *40*, 6990–6995.
[27] G. He, Y. Gu, S. He, U. Schröder, S. Chen, H. Hou, *Bioresour. Technol.* **2011**, *102*, 10763–10766.
[28] D. Pocaznoi, A. Calmet, L. Etcheverry, B. Erable, A. Bergel, *Energy Environ. Sci.* **2012**, *5*, 9645–9652.
[29] B. E. Logan, J. M. Regan, *Environ. Sci. Technol.* **2006**, *40*, 5181–5192.

[30] A. Kato Marcus, C. I. Torres, B. E. Rittmann, *Biotechnol. Bioeng.* **2007**, *98*, 1171 – 1182.

[31] H. V. M. Hamelers, A. Ter Heijne, N. Stein, R. A. Rozendal, C. J. N. Buisman, *Bioresour. Technol.* **2011**, *102*, 381 – 387.

[32] J. Bard, L. R. Faulkner, *Electrochemical Methods, 2nd ed.*, John Wiley & Sons, New York, **2001**, ch. 3, p. 97.

[33] L. Pons, M.-L. Délia, A. Bergel, *Bioresour. Technol.* **2011**, *102*, 2678 – 2683.

[34] J. Hong, H. Ghourchian, A. A. Moosavi-Movahedi, *Electrochem. Commun.* **2006**, *8*, 1572 – 1576.

[35] M. F. J. M. Verhagen, W. R. Hagen, *J. Electroanal. Chem.* **1992**, *334*, 339 – 350.

[36] S. F. Wang, T. Chen, Z. L. Zhang, X. C. Shen, Z. X. Lu, D. W. Pang, K. Y. Wong, *Langmuir* **2005**, *21*, 9260 – 9266.

[37] S. T. Read, P. Dutta, P. L. Bond, J. Keller, K. Rabaey, *BMC Microbiol.* **2010**, *10*, 98.

[38] M. Speers, G. Reguera, *Appl. Environ. Microbiol.* **2012**, *78*, 437 – 444.

[39] A. Chavez-Dozal, M. K. Nishiguchi, *J. Basic Microbiol.* **2011**, *51*, 452 – 458.

[40] W. Qurashi, A. N. Sabri, *J. Basic Microbiol.* **2012**, *52*, 566 – 572.

[41] J. K. Knobloch, K. Bartscht, A. Sabottke, H. Rohde, H. H. Feucht, D. Mack, *J. Bacteriol.* **2001**, *183*, 2624 – 2633.

[42] D. Janjaroen, F. Ling, G. Monroy, N. Derlon, E. Mogenroth, S. A. Boppart, W.-T. Liu, T. H. Nguyen, *Water Res.* **2013**, *47*, 2531 – 2542.

[43] R. Bond, D. E. Holmes, L. M. Tender, D. R. Lovley, *Science* **2002**, *295*, 483 – 485.

[44] E. Reimers, P. Girguis, H. A. Stecher, L. M. Tender, N. Ryckelynck, P. Whaling, *Geobiology* **2006**, *4*, 123 – 136.

[45] T. Zhang, T. S. Bain, M. A. Barlett, S. A. Dar, O. L. Snoeyenbos-West, K. P. Nevin, D. R. Lovley, *Microbiology* **2014**, *160*, 123 – 129.

[46] S. F. Ketep, A. Bergel, M. Bertrand, W. Achouak, E. Fourest, *Bioresour. Technol.* **2013**, *127*, 448 – 455.

[47] E. Lojou, P. Bianco, M. Bruschi, *Electrochim. Acta* **1998**, *43*, 2005 – 2013.

[48] S. Alves, C. M. Paquete, B. M. Fonseca, R. O. Louro, *Metallomics* **2011**, *3*, 349 – 353.

[49] V. V. Homann, K. J. Edwards, E. A. Webb, A. Butler, *Biometals* **2009**, *22*, 565 – 571.

[50] Y. Zuo, D. Xing, J. M. Regan, B. E. Logan, *Appl. Environ. Microbiol.* **2008**, *74*, 3130 – 3137.

[51] J. Y. He, X. Z. Liu, R. T. Zhao, F. W. Wu, J. X. Wang, *Biodiversity Sci.* **2013**, *21*, 28 – 37.

[52] M. J. Gauthier, B. Lafay, R. Christen, L. Fernandez, M. Acquaviva, P. Bonin, J.-C. Bertrand, *Int. J. Syst. Bacteriol.* **1992**, *42*, 568 – 576.

[53] J. J. Godon, E. Zumstein, P. Dabert, F. Habouzit, R. Moletta, *Appl. Environ. Microbiol.* **1997**, *63*, 2802 – 2813.

[54] C. Delbès, R. Moletta, J. J. Godon, *Environ. Microbiol.* **2000**, *2*, 506 – 515.

[55] N. Wery, V. Bru-Adan, C. Minervini, J. P. Delgenes, L. Garrelly, J. J. Godon, *Appl. Environ. Microbiol.* **2008**, *74*, 3030 – 3037.

[56] R. J. Michelland, S. Dejean, S. Combes, L. Lamothe, L. Cauquil, *Mol. Ecol. Resour.* **2009**, *9*, 1359 – 1363.